

## Electronic Supplementary Information (ESI) for

# Anisotropic Li<sup>+</sup> ion conductivity in a large single crystal of a Co(III) coordination complex

Saet Byeol Kim,<sup>†,§</sup> Jeung Yoon Kim,<sup>‡,§</sup> Nak Cheon Jeong,<sup>\*,‡</sup> and Kang Min Ok<sup>\*,†</sup>

<sup>†</sup>Department of Chemistry, Chung-Ang University, Seoul 06974, Korea

<sup>‡</sup>Department of Emerging Materials Science, DGIST, Daegu 42988, Korea

\*E-mail: kmok@cau.ac.kr (KMO); nc@dgist.ac.kr (NCJ).

### Table of contents

Sections	Titles	pages
Section S1.	Materials and Methods	S2–S4
Section S2.	Crystal Structures of ACo(PDC) <sub>2</sub> (A = Na <sup>+</sup> , K <sup>+</sup> , and H <sub>3</sub> O <sup>+</sup> )	S5–S7
Section S3.	PXRD data of ACo(PDC) <sub>2</sub> (A = Li <sup>+</sup> , Na <sup>+</sup> , K <sup>+</sup> , and H <sub>3</sub> O <sup>+</sup> )	S8
Section S4.	Spectroscopic Characterization of ACo(PDC) <sub>2</sub> (A = Li <sup>+</sup> , Na <sup>+</sup> , K <sup>+</sup> , and H <sub>3</sub> O <sup>+</sup> ): Nuclear Magnetic Resonance and Infrared Spectra	S9–S11
Section S5.	Thermal Analyses of ACo(PDC) <sub>2</sub> (A = Li <sup>+</sup> , Na <sup>+</sup> , K <sup>+</sup> , and H <sub>3</sub> O <sup>+</sup> )	S12–S13
Section S6.	Conductivity Measurements of LiCo(PDC) <sub>2</sub> Single Crystal along the [100] and [001] Directions	S14
Section S7.	Orientation of LiCo(PDC) <sub>2</sub> Crystals in Pellet Sample	S15
Section S8.	Redox Potentials and Conductivity Test of LiCo(PDC) <sub>2</sub>	S16–S18
Section S9.	Conductivity Measurements of ACo(PDC) <sub>2</sub> (A = Na <sup>+</sup> , K <sup>+</sup> , and H <sub>3</sub> O <sup>+</sup> ) Single Crystals	S19
Section S10.	Identification of Conductivity in LiCo(PDC) <sub>2</sub>	S20
Section S11.	Temperature-dependent Conductivity Measurements for LiCo(PDC) <sub>2</sub>	S21
References		S22

## Section S1. Materials and Methods

**Materials.** All reagents were obtained from commercial sources (Sigma Aldrich or Alfa Aesar) and were used without further purification. Cobalt(II) nitrate hexahydrate ( $\text{Co}(\text{NO}_3)_2 \cdot 6\text{H}_2\text{O}$ , Aldrich, 98%), lithium nitrate ( $\text{LiNO}_3$ , Aldrich,  $\geq 99\%$ ), sodium nitrate ( $\text{NaNO}_3$ , Aldrich,  $\geq 99\%$ ), potassium nitrate ( $\text{KNO}_3$ , Aldrich,  $\geq 99\%$ ), 2,6-pyridine-dicarboxylic acid (PDC,  $\text{C}_7\text{H}_5\text{NO}_4$ , Alfa Aesar, 98%), nitric acid ( $\text{HNO}_3$ , Aldrich,  $>70\%$ ), and distilled deionized water (DDW) were used for syntheses of Cobalt-PDC complexes in both single crystals and polycrystalline phases. Silver pastes (16040-30 fast-drying Ag paint, TED PELLA for microelectrodes; type A and B, Chemtronix for pellet samples) and copper wires (SPCP-001-500, diameter = 0.01 mm, OMEGA Engineering for microelectrodes; tin-coated copper wires, diameter = 0.25 mm, Arcor, for pellet samples) were used to prepare electrodes connected to single-crystal and pellet samples.

**Syntheses of polycrystalline  $\text{ACo}(\text{PDC})_2$  ( $\text{A} = \text{Li}^+$ ,  $\text{Na}^+$ ,  $\text{K}^+$ , and  $\text{H}_3\text{O}^+$ ).** A 1.0 mmol portion of  $\text{Co}(\text{NO}_3)_2$  (0.291 g) and 1.0 mmol of PDC (0.334 g) were dissolved in 1 mL of DDW. After continuous stirring for 30 min at room temperature, 0.5 mL of  $\text{HNO}_3$  was added to the mixed solution. The transparent solution was introduced into a Teflon-lined autoclave and placed in an oven at 180 °C for 3 days. After cooling to room temperature, pure polycrystalline samples of  $[\text{H}_3\text{O}^+]\text{Co}(\text{PDC})_2$  were isolated by filtration. Polycrystalline samples of  $\text{LiCo}(\text{PDC})_2$ ,  $\text{NaCo}(\text{PDC})_2$ , and  $\text{KCo}(\text{PDC})_2$  were also synthesized by the same synthetic procedures, with the substitution of 1.0 mmol of the respective  $\text{MNO}_3$  ( $\text{M} = \text{Li}$ ,  $\text{Na}$ , or  $\text{K}$ ) in place of  $\text{HNO}_3$ . Table S1 summarizes the elemental microanalysis data for all title compounds.

**Table S1.** C, H, and N Content in  $\text{ACo}(\text{PDC})_2$  ( $\text{A} = \text{Li}^+$ ,  $\text{Na}^+$ ,  $\text{K}^+$ , and  $\text{H}_3\text{O}^+$ )

Sample	Carbon (%)		Hydrogen (%)		Nitrogen (%)	
	observed	calculated	observed	calculated	observed	calculated
$[\text{H}_3\text{O}^+]\text{Co}(\text{PDC})_2$	41.29	41.30	1.98	1.98	6.84	6.88
$\text{LiCo}(\text{PDC})_2$	38.29	38.71	2.32	2.38	6.35	6.45
$\text{NaCo}(\text{PDC})_2$	37.53	37.52	2.21	2.25	6.25	6.25
$\text{KCo}(\text{PDC})_2$	39.23	39.27	1.52	1.41	6.60	6.54

**Syntheses of  $\text{ACo}(\text{PDC})_2$  ( $\text{A} = \text{Li}^+$ ,  $\text{Na}^+$ ,  $\text{K}^+$ , and  $\text{H}_3\text{O}^+$ ) single crystals.** Large single crystals of  $\text{ACo}(\text{PDC})_2$  ( $\text{A} = \text{Li}^+$ ,  $\text{Na}^+$ ,  $\text{K}^+$ , and  $\text{H}_3\text{O}^+$ ) were grown using procedures similar to the one described above, except that the amount of water was increased to 8 mL. To synthesize  $[\text{H}_3\text{O}^+]\text{Co}(\text{PDC})_2$  single crystals, a 1.0 mmol portion of  $\text{Co}(\text{NO}_3)_2$  (0.291 g) and 1.0 mmol of PDC (0.334 g) were dissolved in 8 mL of DDW. After continuous stirring for 30 min at room temperature, 0.5 mL of  $\text{HNO}_3$  was added to the mixed solution. The transparent solution was introduced into a Teflon-lined autoclave and placed in an oven at 180 °C for 3 days. After cooling to room temperature, the solvent was slowly evaporated under ambient conditions for several days. Single crystals of  $\text{LiCo}(\text{PDC})_2$ ,  $\text{NaCo}(\text{PDC})_2$ , and  $\text{KCo}(\text{PDC})_2$  were also grown by the same procedure, with the substitution of 1.0 mmol of the respective  $\text{MNO}_3$  ( $\text{M} = \text{Li}$ ,  $\text{Na}$ , or  $\text{K}$ ) in place of  $\text{HNO}_3$ . The crystal structures of all title compounds were determined by single-crystal X-ray diffraction (see below).

**Preparation of pellets for conductivity measurements of  $\text{LiCo(PDC)}_2$ .** Pellets for the conductivity measurements of  $\text{LiCo(PDC)}_2$  were prepared with a thickness of ca. 2 mm by pressing polycrystalline samples in a pellet die (7 mm diameter) under a pressure of ca. 1 metric ton. The flat sides of the prepared pellets were connected electrically to an impedance spectrometer (or DC potentiostat) using tin-coated copper wires (diameter = 0.25 mm, Arcor) and conductive silver epoxy (type A and B, Chemtronix). Conductivity measurements were performed under ambient conditions at room temperature (ca. 20 °C) without supplying solvent or electrolyte.

**Preparation of microelectrodes for conductivity measurements of single crystals.** To examine the ionic conduction behaviors of  $\text{ACo(PDC)}_2$  crystals ( $A = \text{Li}^+, \text{Na}^+, \text{K}^+, \text{and } \text{H}_3\text{O}^+$ ), crystals of  $\text{LiCo(PDC)}_2$  ( $0.88 \times 1.97 \times 0.63 \text{ mm}^3$ ),  $\text{NaCo(PDC)}_2$  ( $0.54 \times 1.36 \times 2.71 \text{ mm}^3$ ),  $\text{KCo(PDC)}_2$  ( $1.40 \times 1.50 \times 0.75 \text{ mm}^3$ ), and  $[\text{H}_3\text{O}]\text{Co(PDC)}_2$  ( $1.05 \times 1.97 \times 0.83 \text{ mm}^3$ ) were connected electrically to an impedance spectrometer using thin copper wires (diameter = 0.01 mm, OMEGA Engineering) and conductive silver paint (TED PELLA). The connections were made along the [100], [010], and [001] axes for all crystals. All conductivity measurements were performed under ambient conditions at room temperature (ca. 20 °C) without supplying solvent or electrolyte. (See Figure S1.)

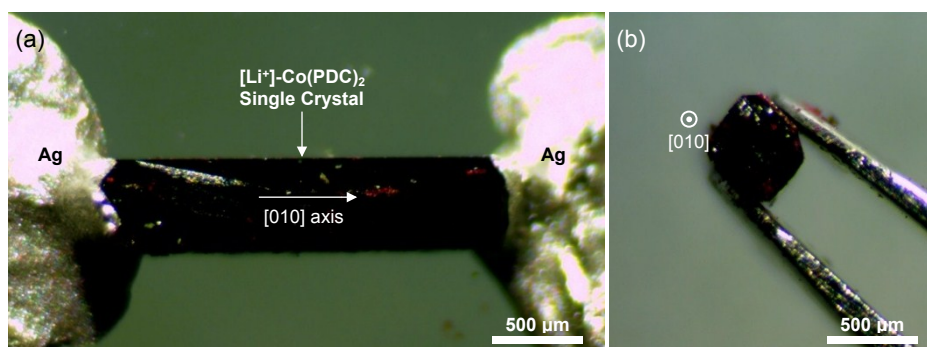


**Figure S1.** Optical microscope images of (a) a  $\text{LiCo(PDC)}_2$  single crystal connected to the silver electrode along the [010] direction and (b) (010) facet.

**Instrumentation.** The crystal structures of the synthesized compounds were determined by a single-crystal X-ray diffraction technique. The data were collected using a Bruker SMART BREEZE diffractometer equipped with a monochromatic graphite-filtered Mo  $K_{\alpha}$  beam. Single crystals of  $\text{LiCo(PDC)}_2$  ( $0.020 \times 0.020 \times 0.133 \text{ mm}^3$ ),  $\text{NaCo(PDC)}_2$  ( $0.026 \times 0.026 \times 0.137 \text{ mm}^3$ ),  $\text{KCo(PDC)}_2$  ( $0.046 \times 0.046 \times 0.106 \text{ mm}^3$ ), and  $[\text{H}_3\text{O}]\text{Co(PDC)}_2$  ( $0.010 \times 0.025 \times 0.048 \text{ mm}^3$ ) were attached to glass fibers. The data were collected at 173 K, exposing the crystal samples to the X-ray beam for 10 seconds at every  $0.3^\circ$  rotation in omega. The collected X-ray intensities were integrated using SAINT software<sup>S1</sup> with correction of polarization, Lorentz factor, and X-ray absorption attributed to air and sample vibration. The structures were solved and refined using the software SHELXS-97<sup>S2</sup> and SHELXL-97,<sup>S3</sup> respectively. All atoms except hydrogen atoms were refined anisotropically. All calculations were performed using the WinGX-98 crystallographic software package.<sup>S4</sup> Crystallographic data for the reported compounds are given in Table S2. The phase purities of the synthesized compounds were examined by powder X-ray diffraction. PXRD patterns of the samples were obtained using a Bruker D8-Advance diffractometer with a monochromatic nickel-filtered Cu  $K_{\alpha}$  beam at room temperature. Infrared spectra of the samples were recorded on a Thermo Scientific iS10 FT-IR spectrometer in attenuated total reflectance (ATR) mode.  $^1\text{H}$  and  $^{13}\text{C}$  NMR spectra were recorded using a Varian VNS spectrometer (600 MHz for  $^1\text{H}$  NMR and 151 MHz for  $^{13}\text{C}$  NMR). The samples were dissolved in  $\text{D}_2\text{O}$  prior to measurement of NMR spectra. Thermal gravimetric analyses (TGA) were performed using a TGA-N 1000 thermal analyzer (Scinco) under flowing argon. Impedance spectra of the single-crystal samples were recorded in the frequency range of  $0.1\text{--}10^7$  using a SI1260 Impedance/Gain-Phase analyzer (Solartron Analytical). Measurements were performed under ambient condition at room temperature (ca.  $20^\circ\text{C}$ ). A microscope (S43T, Microscopes Inc.) was used in the process of sample preparation for impedance tests. The DDW used as the solvent in the syntheses of crystalline compounds was obtained from a water purification system (Merck Millipore, MQ Direct 8).

## Section S2. Crystal Structures of ACo(PDC)<sub>2</sub> (A = Na<sup>+</sup>, K<sup>+</sup>, and H<sub>3</sub>O<sup>+</sup>)

NaCo(PDC)<sub>2</sub> is a molecular compound that crystallizes in the monoclinic space group *P*2<sub>1</sub>/*c* (No. 14). The structure of NaCo(PDC)<sub>2</sub> comprises a Co<sup>3+</sup> cation, two PDC ligands, and the Na<sup>+</sup> cation. The unique Co<sup>3+</sup> cation is surrounded by two N and four O atoms in the PDC ligands in the octahedral coordination environment. The Co–N and Co–O bond distances are in the ranges of 1.8392(15)–1.8439(16) and 1.9062(13)–1.9175(14) Å, respectively. As shown in Figures S2a and b, the PDC ligands in NaCo(PDC)<sub>2</sub> are aligned approximately parallel along the *b* and *c* axes due to π–π interactions. The observed distances of the two parallel pyridine rings are approximately 3.6 Å. The unique Na<sup>+</sup> cation interacts with two water molecules and four oxygen atoms in the carboxylate of the PDC ligands with Na–O contact lengths of 2.2889(18)–2.7852(17) Å.

KCo(PDC)<sub>2</sub> and (H<sub>3</sub>O)Co(PDC)<sub>2</sub> are isostructural molecular compounds that crystallize in the highly symmetric tetragonal space group *I*4<sub>1</sub>/*a* (No. 88). Thus, only the structural details of KCo(PDC)<sub>2</sub> will be provided here. The structure of KCo(PDC)<sub>2</sub> consists of a Co<sup>3+</sup> cation, two PDC ligands, and a K<sup>+</sup> cation. The unique Co<sup>3+</sup> cation is in a six-coordinate distorted octahedral coordination environment with four O and two N atoms. The observed Co–O and Co–N bond distances are 1.922(2) and 1.839(4) Å, respectively. The carboxylate groups of the PDC ligand are connected to the Co<sup>3+</sup> cation through the oxygen atom, O(1). The C(4)–O(1) and C(4)–O(2) bond lengths in the carboxylate groups of the 2,6-PDC ligands are 1.303(4) Å and 1.229(4) Å, respectively. Figure S2c presents a ball-and-stick and polyhedral representation of KCo(PDC)<sub>2</sub> in the *ac* plane. Interestingly, the PDC ligands are aligned approximately parallel to each other along the *a* and *b* axes. The observed distances between the two parallel pyridine rings of the PDC ligands are approximately 3.57 Å (see Figure S2c). The close contact distances indicate that significant parallel π–π interactions exist between the pyridine rings, although the rings are slightly deviated. The K<sup>+</sup> ions are located between the Co-coordination compound. The observed K(1)–O(1) and K(1)–O(2) interaction lengths are 3.161(2) and 2.667(2) Å, respectively (see Figure S2d).

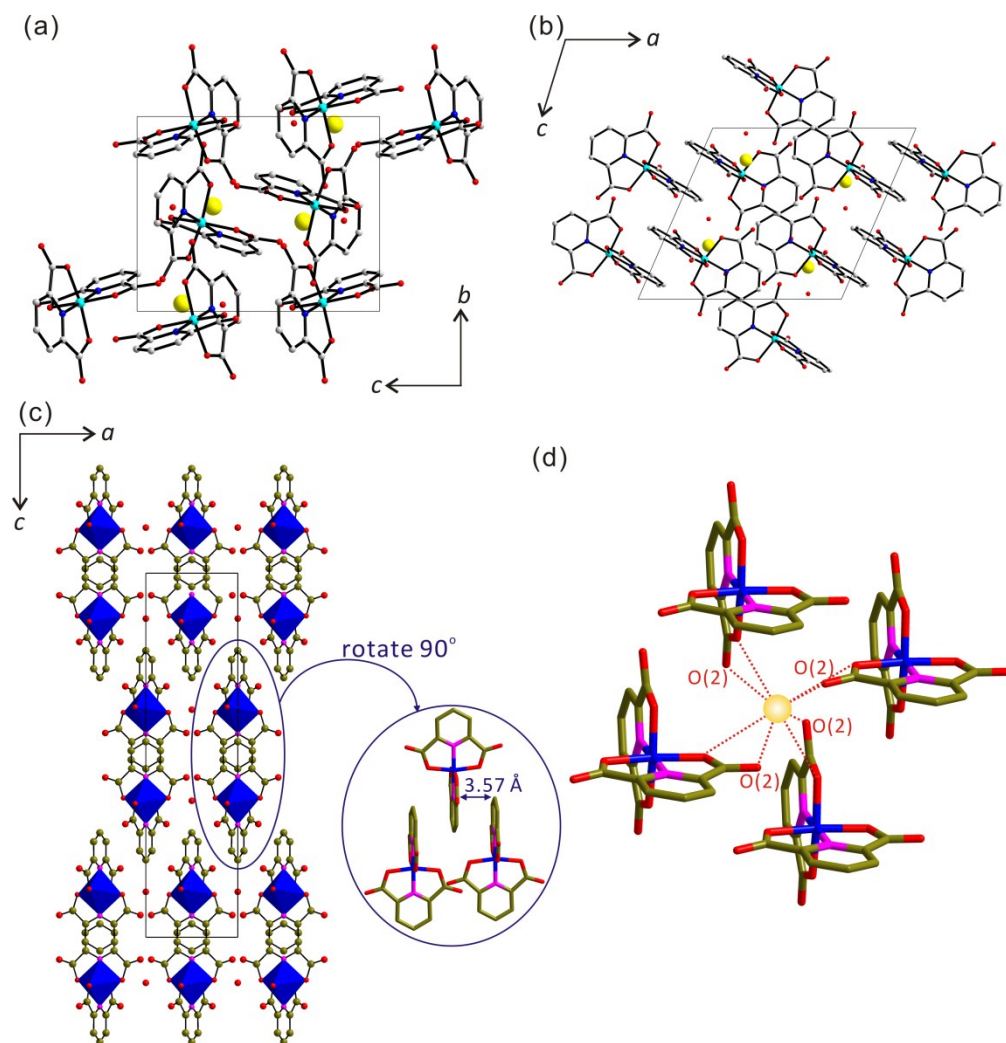


**Figure S2.** Ball-and-stick representations of NaCo(PDC)<sub>2</sub> in the (a) *bc* plane and (b) *ac* plane. (c) Ball-and-stick and polyhedral model of KCo(PDC)<sub>2</sub> in the *ac* plane. (d) The K<sup>+</sup> ions are located between the Co-coordination compounds and interact with eight oxygen atoms. All hydrogen atoms are omitted for clarity.

**Table S2. Crystallographic Data for ACo(PDC)<sub>2</sub> (A = Li, Na, K, and H<sub>3</sub>O)**

<i>Compound</i>	LiCo(PDC) <sub>2</sub>	NaCo(PDC) <sub>2</sub>	KCo(PDC) <sub>2</sub>	[H <sub>3</sub> O]Co(PDC) <sub>2</sub>
<i>fw</i>	3474.90	448.16	428.24	407.15
<i>crystal system</i>	Monoclinic	Monoclinic	Tetragonal	Tetragonal
<i>space group</i>	<i>I</i> 2/ <i>a</i> (no. 15)	<i>P</i> 2 <sub>1</sub> / <i>c</i> (no. 14)	<i>I</i> 4 <sub>1</sub> / <i>a</i> (no. 88)	<i>I</i> 4 <sub>1</sub> / <i>a</i> (no. 88)
<i>a</i> (Å)	21.3041(3)	14.0209(10)	6.9113(10)	7.0260(10)
<i>b</i> (Å)	14.3738(2)	9.5023(10)	6.9113(10)	7.0260(10)
<i>c</i> (Å)	21.3818(3)	12.8892(10)	28.4262(14)	27.891(3)
<i>α</i> (°)	90	90	90	90
<i>β</i> (°)	92.286(10)	113.564(10)	90	90
<i>γ</i> (°)	90	90	90	90
<i>V</i> (Å <sup>3</sup> )	6542.34(14)	1574.1(3)	1357.8(4)	1376.8(4)
<i>Z</i>	2	4	4	4
<i>λ</i> (Å)	0.71073	0.71073	0.71073	0.71073
<i>T</i> (K)	173.0(2)	173.0(2)	173.0(2)	173.0(2)
<i>ρ</i> <sub>calcd</sub> (g·cm <sup>-3</sup> )	1.764	1.891	2.095	1.964
<i>R</i> ( <i>F</i> ) <sup>a</sup>	0.0370	0.0305	0.0397	0.0262
<i>R</i> <sub>w</sub> ( <i>R</i> <sub>o</sub> <sup>2</sup> ) <sup>b</sup>	0.0738	0.0695	0.1023	0.0706

$$^a R(F) = \sum ||F_o| - |F_c|| / \sum |F_o|.$$

$$^b R_w(F_o^2) = [\sum w(F_o^2 - F_c^2)^2 / \sum w(F_o^2)^2]^{1/2}.$$

### Accession Codes

CCDC 1476207–1476210 contain the supplementary crystallographic data for this paper. These data can be obtained free of charge via [www.ccdc.cam.ac.uk/data\\_request/cif](http://www.ccdc.cam.ac.uk/data_request/cif), or by emailing [data\\_request@ccdc.cam.ac.uk](mailto:data_request@ccdc.cam.ac.uk), or by contacting The Cambridge Crystallographic Data Centre, 12 Union Road, Cambridge CB2 1EZ, UK; fax: +44 1223 336033.

### Section S3. PXRD data of $\text{ACo(PDC)}_2$ ( $\text{A} = \text{Li}^+, \text{Na}^+, \text{K}^+, \text{and } \text{H}_3\text{O}^+$ )

Powder X-ray diffraction (PXRD) patterns of  $\text{ACo(PDC)}_2$  ( $\text{A} = \text{Li}^+, \text{Na}^+, \text{K}^+, \text{and } \text{H}_3\text{O}^+$ ) were obtained to confirm the phase purity of the synthesized compounds. The measured PXRD patterns were consistent with the data calculated from single-crystal diffraction (see Figure S3).

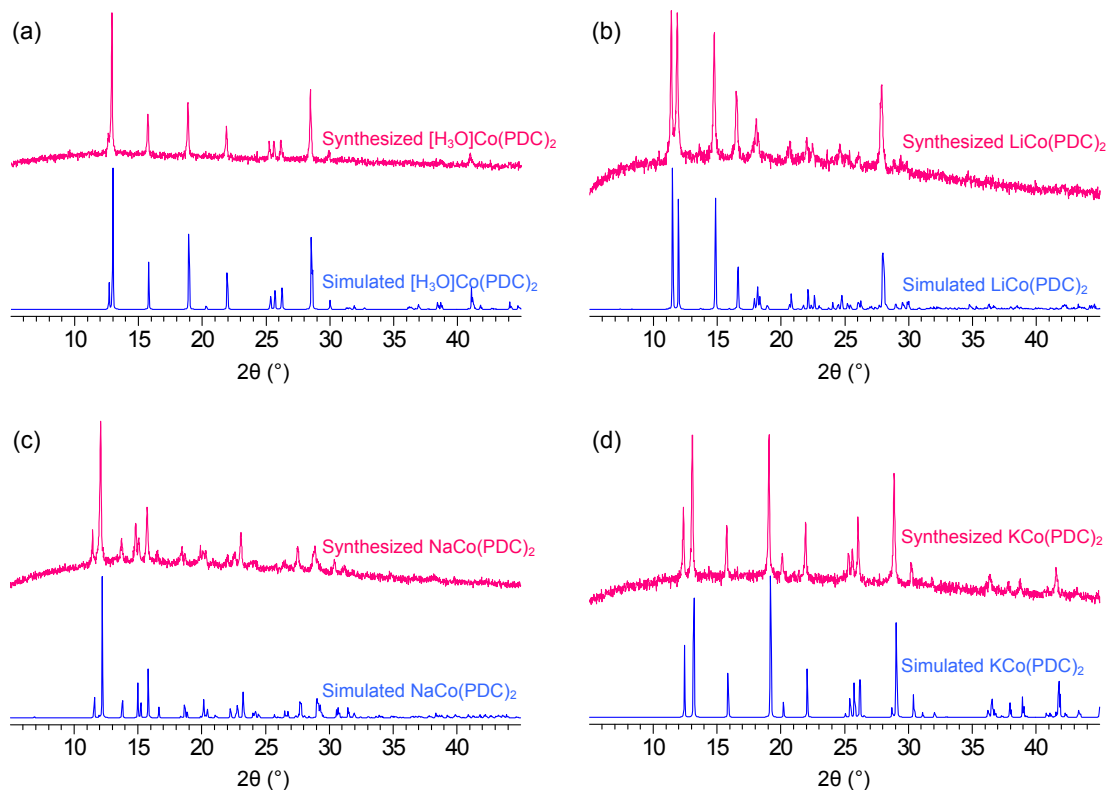


**Figure S3.** Experimental (red) and calculated (blue) PXRD patterns of (a)  $[\text{H}_3\text{O}]\text{Co(PDC)}_2$ , (b)  $\text{LiCo(PDC)}_2$ , (c)  $\text{NaCo(PDC)}_2$ , and (d)  $\text{KCo(PDC)}_2$ .



## Section S4. Spectroscopic Characterization of $\text{ACo}(\text{PDC})_2$ ( $\text{A} = \text{Li}^+, \text{Na}^+, \text{K}^+, \text{and } \text{H}_3\text{O}^+$ ): Nuclear Magnetic Resonance and Infrared Spectra

To characterize the molecular structures of the synthesized crystals, nuclear magnetic resonance (NMR) and infrared (IR) spectroscopic data were obtained (see Figures S4 and S5, and Tables S3 and S4). The obtained spectra agreed well with the structures obtained from single-crystal X-ray diffraction. The vibration frequencies of  $\text{Co}-\text{O}$  and  $\text{Co}-\text{N}$  at ca.  $665$  and  $590 \text{ cm}^{-1}$  in the IR spectra agree well with reported values in the literature (see Figure S5 and Table S4).<sup>S5-S6</sup>

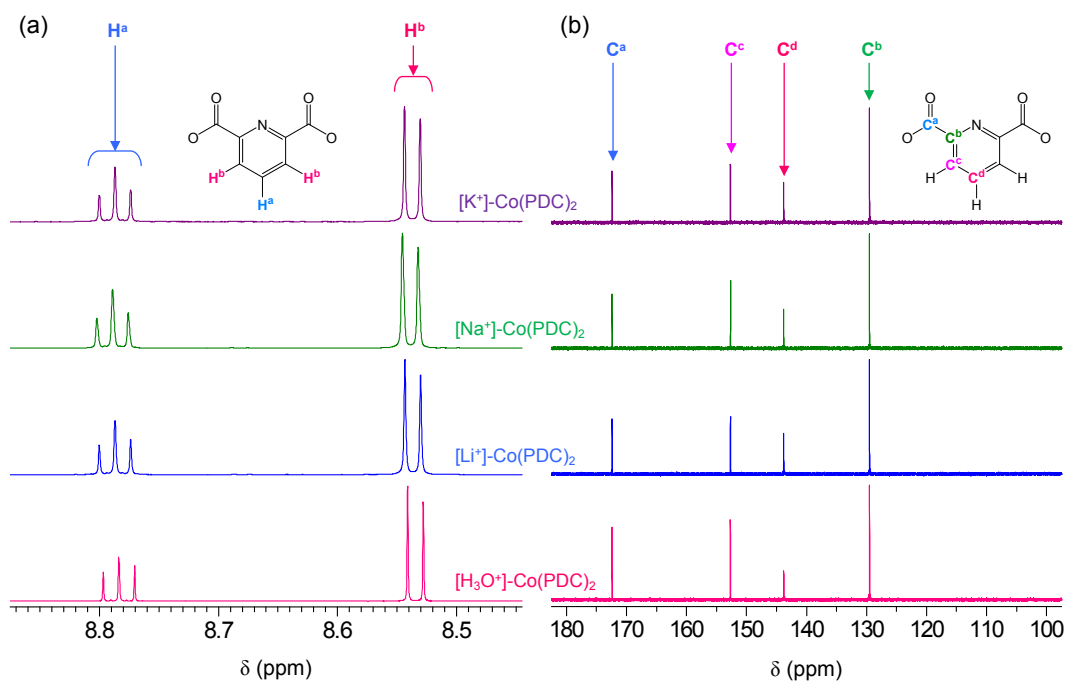


**Figure S4.** (a)  $^1\text{H}$  and (b)  $^{13}\text{C}$  NMR spectra of the  $[\text{H}_3\text{O}^+]\text{Co}(\text{PDC})_2$ ,  $\text{LiCo}(\text{PDC})_2$ ,  $\text{NaCo}(\text{PDC})_2$ , and  $\text{KCo}(\text{PDC})_2$  complexes. The complexes were dissolved in  $\text{D}_2\text{O}$  for the measurements.

**Table S3.** Characteristic Chemical Shifts of  $[\text{H}_3\text{O}]\text{Co}(\text{PDC})_2$ ,  $\text{LiCo}(\text{PDC})_2$ ,  $\text{NaCo}(\text{PDC})_2$ , and  $\text{KCo}(\text{PDC})_2$  in  $^1\text{H}$  and  $^{13}\text{C}$  NMR Spectra

Compound	$^1\text{H}$ -NMR			$^{13}\text{C}$ -NMR	
	H atom	Chemical shift (ppm)	Integration ratio	C atom	Chemical shift (ppm)
$[\text{H}_3\text{O}]\text{Co}(\text{PDC})_2$	$\text{H}^a$	8.797	1.0	$\text{C}^a$	172.4
		8.784		$\text{C}^b$	129.5
		8.770		$\text{C}^c$	152.7
	$\text{H}^b$	8.541	1.9	$\text{C}^d$	143.8
		8.528		-	-
$\text{LiCo}(\text{PDC})_2$	$\text{H}^a$	8.800	1.0	$\text{C}^a$	172.4
		8.787		$\text{C}^b$	129.5
		8.774		$\text{C}^c$	152.7
	$\text{H}^b$	8.543	1.9	$\text{C}^d$	143.8
		8.530		-	-
$\text{NaCo}(\text{PDC})_2$	$\text{H}^a$	8.802	1.0	$\text{C}^a$	172.4
		8.789		$\text{C}^b$	129.5
		8.776		$\text{C}^c$	152.7
	$\text{H}^b$	8.546	1.8	$\text{C}^d$	143.8
		8.532		-	-
$\text{KCo}(\text{PDC})_2$	$\text{H}^a$	8.800	1.0	$\text{C}^a$	172.4
		8.787		$\text{C}^b$	129.5
		8.774		$\text{C}^c$	152.7
	$\text{H}^b$	8.544	1.8	$\text{C}^d$	143.8
		8.831		-	-

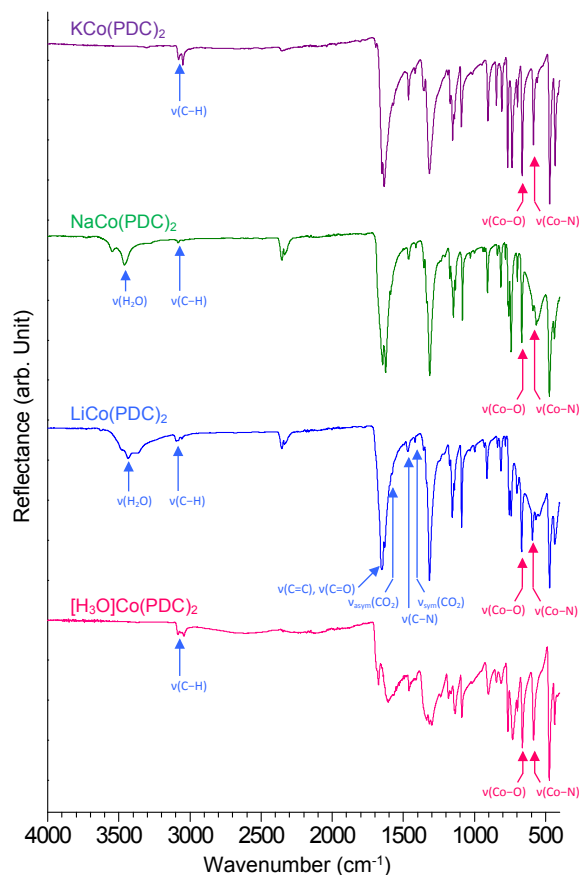


**Figure S5.** Infrared spectra of  $[\text{H}_3\text{O}]\text{Co}(\text{PDC})_2$ ,  $\text{LiCo}(\text{PDC})_2$ ,  $\text{NaCo}(\text{PDC})_2$ , and  $\text{KCo}(\text{PDC})_2$ .

**Table S4.** Vibration Frequencies of Characteristic Chemical Bonds in the  $[\text{H}_3\text{O}]\text{Co}(\text{PDC})_2$ ,  $\text{LiCo}(\text{PDC})_2$ ,  $\text{NaCo}(\text{PDC})_2$ , and  $\text{KCo}(\text{PDC})_2$  Complexes

Vibration mode	Vibration frequencies ( $\text{cm}^{-1}$ )			
	$[\text{H}_3\text{O}]\text{Co}(\text{PDC})_2$	$\text{LiCo}(\text{PDC})_2$	$\text{NaCo}(\text{PDC})_2$	$\text{KCo}(\text{PDC})_2$
$\nu(\text{H}_2\text{O})$		3490–3360	3545–3460	
$\nu(\text{C-H})$	3090–3040	3100–3050	3090–3040	3090–3040
$\nu(\text{C=C}), \nu(\text{C=O})$	1675–1605	1675–1630	1670–1620	1660–1620
$\nu(\text{antisymmetric CO}_2)$	1605–1580	1605–1570	1620–1560	1620–1550
$\nu(\text{C-N})$	1460	1470	1460	1465
$\nu(\text{symmetric CO}_2)$	1410	1417	1410	1415
$\nu(\text{Co-O})$	663	668	667	664
$\nu(\text{Co-N})$	585	594	589	585

## Section S5. Thermal Analyses of $\text{ACo(PDC)}_2$ ( $\text{A} = \text{Li}^+, \text{Na}^+, \text{K}^+, \text{and H}_3\text{O}^+$ )

To investigate the thermal stability of the reported materials,  $\text{ACo(PDC)}_2$  ( $\text{A} = \text{H}_3\text{O}^+, \text{Li}^+, \text{Na}^+, \text{and K}^+$ ), thermogravimetric analyses (TGA) and PXRD were performed. The TGA data for  $[\text{H}_3\text{O}]\text{Co(PDC)}_2$  revealed that weight loss begins at a relatively high temperature of ca. 260 °C (see Figure S6). For  $\text{KCo(PDC)}_2$ , decomposition also begins at ca. 320 °C. We speculate that these high decomposition temperatures can be attributed to the strong binding of the  $\text{H}_3\text{O}^+$  and  $\text{K}^+$  ions to neighboring oxygen atoms in the PDC ligands. The TGA diagrams of  $\text{LiCo(PDC)}_2$  and  $\text{NaCo(PDC)}_2$  exhibit weight loss at lower temperatures of ca. 150 °C and 100 °C, respectively, due to the loss of occluded water molecules.

The presence of alkali metal ions in the samples was corroborated by examining the PXRD patterns for the calcined products. The resulting patterns agreed well with the simulated PXRD patterns of the corresponding oxides, such as  $\text{Co}_3\text{O}_4$ ,  $\text{LiCoO}_2$ ,  $\text{Na}_{0.5}\text{CoO}_2$ ,  $\text{NaCoO}_2$ , and  $\text{KCoO}_2$  (see Figure S7).

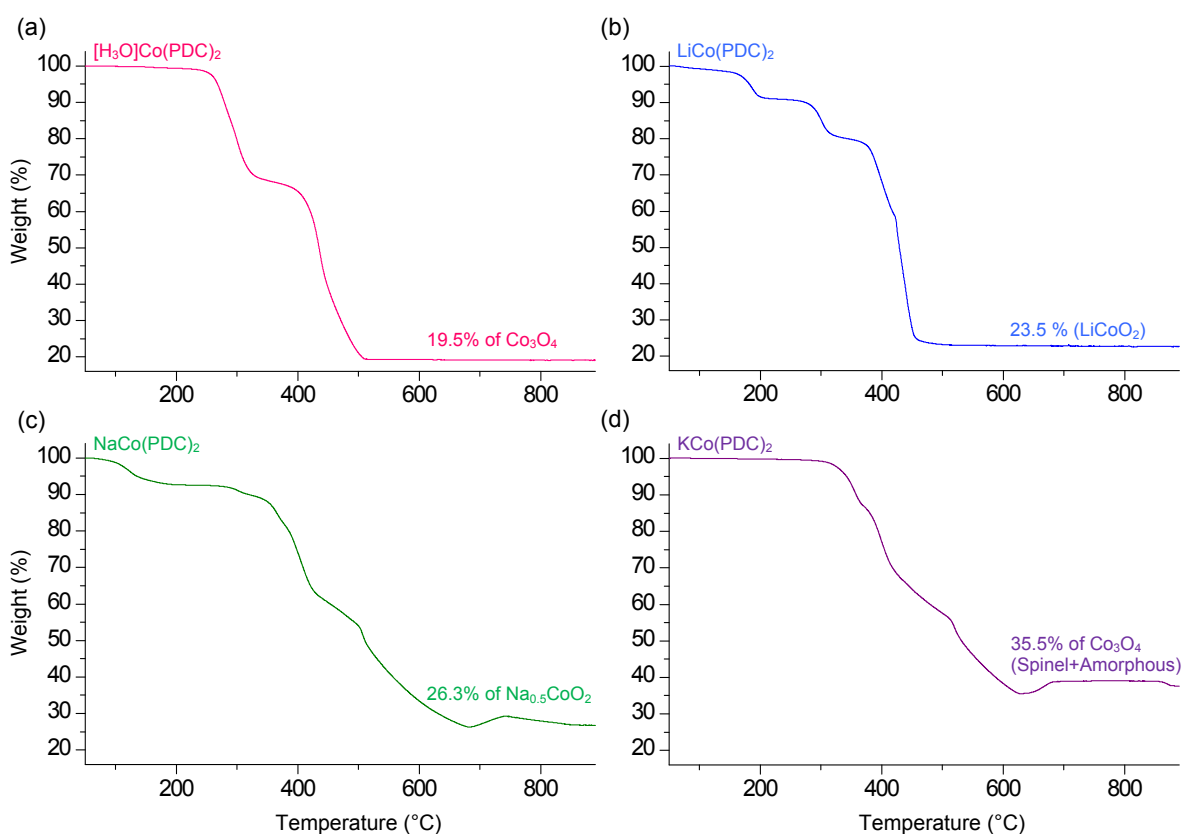


**Figure S6.** TGA diagrams of (a)  $[\text{H}_3\text{O}]\text{Co(PDC)}_2$ , (b)  $\text{LiCo(PDC)}_2$ , (c)  $\text{NaCo(PDC)}_2$ , and (d)  $\text{KCo(PDC)}_2$ .

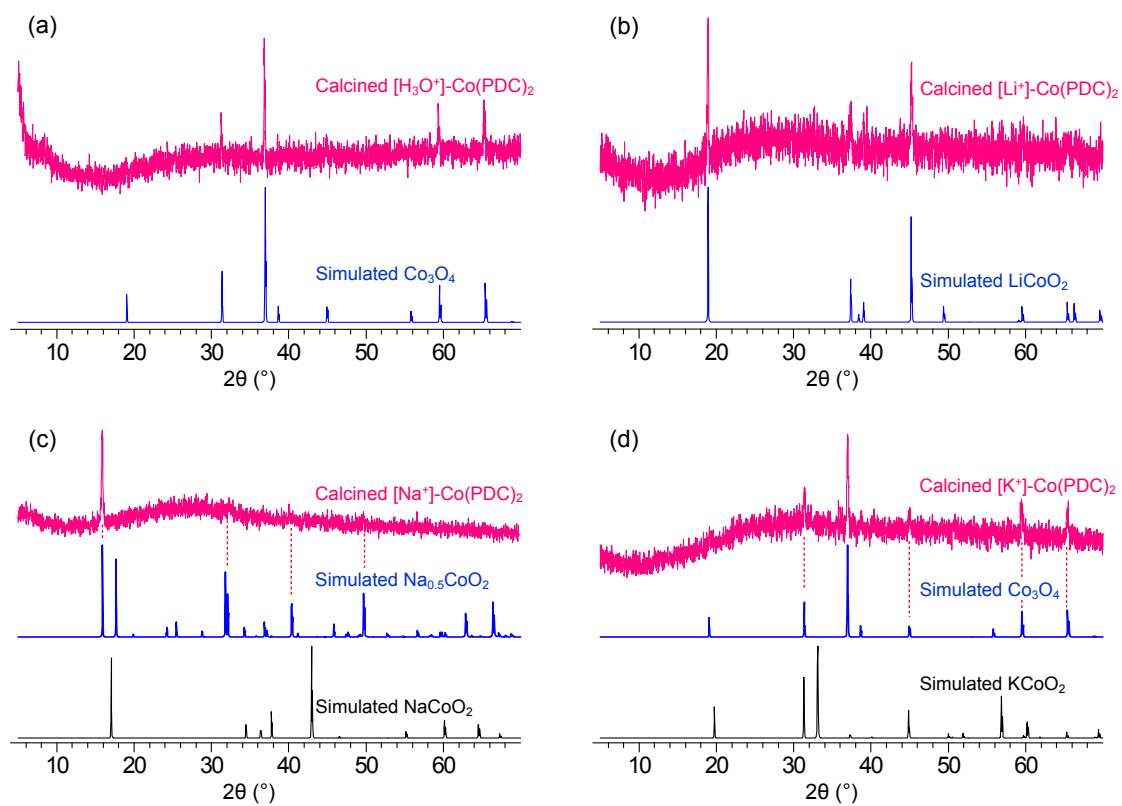


**Figure S7.** PXRD patterns (red) of the powders obtained after calcination of (a) [H<sub>3</sub>O]Co(PDC)<sub>2</sub>, (b) LiCo(PDC)<sub>2</sub>, (c) NaCo(PDC)<sub>2</sub>, and (d) KCo(PDC)<sub>2</sub> at 800 °C. The blue and black patterns represent the simulated PXRD results for (a) Co<sub>3</sub>O<sub>4</sub>, (b) LiCoO<sub>2</sub>, (c) Na<sub>0.5</sub>CoO<sub>2</sub> and NaCoO<sub>2</sub>, and (d) Co<sub>3</sub>O<sub>4</sub> and KCoO<sub>2</sub>.

## Section S6. Conductivity Measurements of $\text{LiCo(PDC)}_2$ Single Crystal along the [100] and [001] Directions

We observed ion conduction behavior of a  $\text{LiCo(PDC)}_2$  single crystal measured along the [010] direction. We attributed this conduction to the presence of ion channels in the direction as a first requisite. We hypothesized that, by contrast, ion conduction is not observed the [100] and [001] directions because of the absence of such ion channels. Based on this hypothesis, we examined whether ion conduction occurs in the [100] and [001] directions. We prepared single crystal samples connected in the directions of [100] and [001] and performed EIS measurements on the samples. As expected, we did not observe an impedance signal. All data in the spectra were scattered completely, indicating a lack of ion conduction in the two directions (see Figure S8).

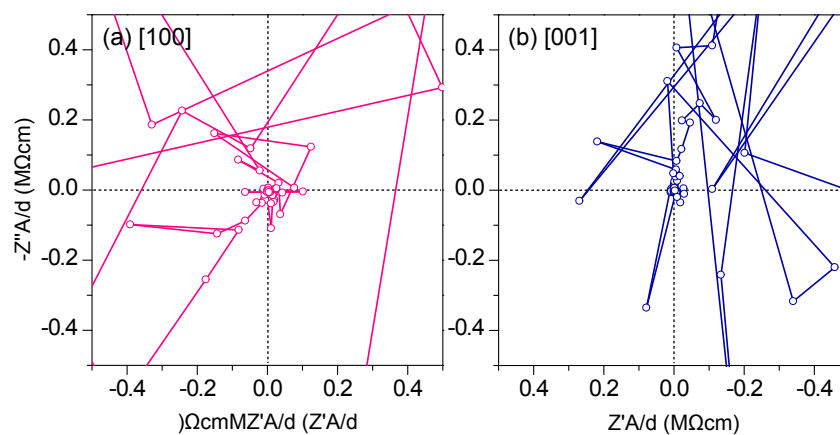


**Figure S8.** Typical impedance spectra of a  $\text{LiCo(PDC)}_2$  single crystal connected in the direction of the (a) [100] and (b) [001] axes.

## Section S7. Orientation of $\text{LiCo}(\text{PDC})_2$ Crystals in Pellet Sample

We wondered if  $\text{LiCo}(\text{PDC})_2$  Crystals in pellet sample are aligned well or randomly oriented. To this end, we examined the PXRD of a pellet sample. For comparison, the diffraction patterns of powder and single crystal samples were also examined. In particular, the PXRD of the single crystal was taken with its specific orientations which are aligned parallel and perpendicular to the axis of goniometer movement, respectively. Whereas the single crystal exhibits specific diffraction peaks, the PXRD pattern of the pellet sample was same as that of the powder sample, in which crystallites must be randomly oriented (see Figure S9). Furthermore, the measured diffraction pattern of the pellet was identical to the simulated pattern of randomly oriented crystals.

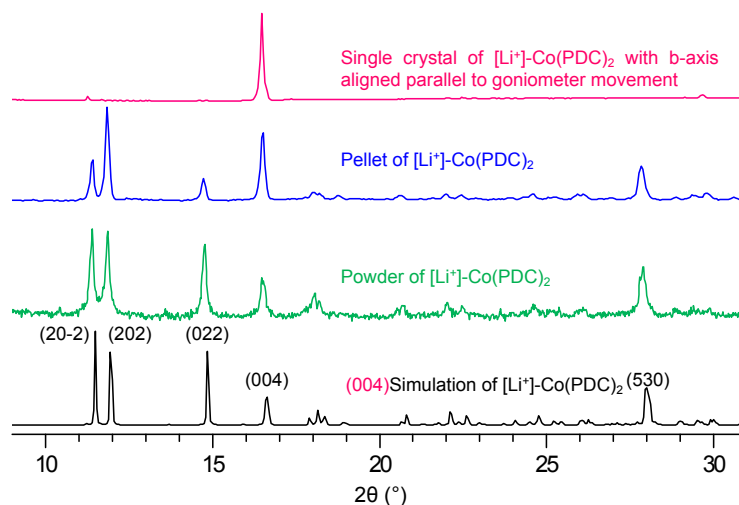


**Figure S9.** XRD patterns of powder, pellet, single crystal samples of  $[\text{Li}^+]\text{-Co}(\text{PDC})_2$ . For comparison, the diffraction pattern of  $[\text{Li}^+]\text{-Co}(\text{PDC})_2$  was also simulated using a Materials Studio software.

## Section S8. Redox Potentials and Conductivity Test of $\text{LiCo}(\text{PDC})_2$

We postulated that the central transition metal ion,  $\text{Co}^{3+}$ , should reversibly interchange its oxidation state to  $\text{Co}^{4+}$  simultaneous with the movement of the interstitial  $\text{Li}^+$  cation to compensate for the instantaneously broken charge balance between the cation and the molecular backbone. Thus, we determined the  $\text{Co}^{3+}/\text{Co}^{4+}$  redox potential by examining a methanol solution containing  $\text{LiCo}(\text{PDC})_2$  by electrochemical cyclic voltammetry (CV). We first dissolved  $\text{LiCo}(\text{PDC})_2$  powder in methanol at a concentration of 0.1 mM. Initially, we attempted to prepare the solution with an aprotic solvent, acetonitrile, to obtain an accurate redox potential by minimizing the solvent effect, but the compound did not dissolve in acetonitrile. Then, we added  $\text{TBABF}_4$  (1 M) to the solution as an additive. The test was performed at a scan rate of  $100 \text{ mV}\cdot\text{s}^{-1}$ .

The recorded CV data indicated two oxidation peaks at ca. -570 and 200 mV (see Figure S10). We attributed the former peak to oxidation from  $\text{Co}^{2+}$  to  $\text{Co}^{3+}$  and the latter to oxidation from  $\text{Co}^{3+}$  to  $\text{Co}^{4+}$  because the observed oxidation potentials were comparable to values reported in the literature within an acceptable range. Because the extraction of the  $\text{Li}^+$  ion from its position should lead to the oxidation of  $\text{Co}^{3+}$  to  $\text{Co}^{4+}$ , we speculate that the transport (or conduction) of the  $\text{Li}^+$  ion occurs at a redox potential of approximately 200 mV. Based on this speculation, we initially acquired the EIS of a  $\text{LiCo}(\text{PDC})_2$  single crystal (aligned to the [010] direction) at a fixed AC potential of 200 mV. However, we varied the DC potentials to 50, 200, and 3,000 mV to monitor a suitable DC potential for ion transport (see Figure S11 and Table S5). The results indicated that transport of  $\text{Li}^+$  ions can be maximized under the conditions of 200 mV DC and 200 mV AC. As expected, although the ion can move under conditions of 50 mV DC and 200 mV AC, the impedance spectra under these conditions were slightly scattered compared to those measured under the above conditions. The impedance spectrum measured at 1,000 mV DC, however, was completely scattered, indicating the absence of ionic conduction in the sample. Based on these results, we performed further EIS experiments with varying AC potentials but fixed DC potential at 200 mV (see the results in Figure 3 of the text).

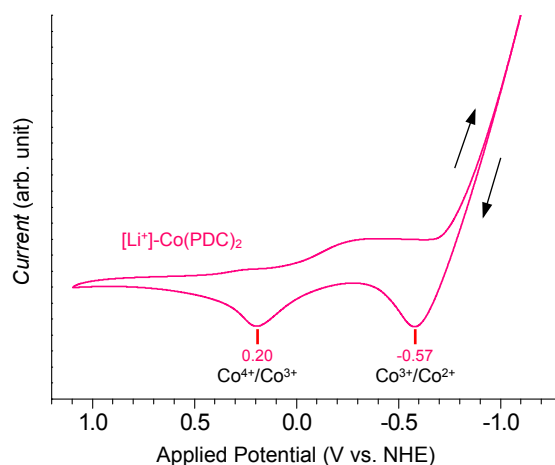


**Figure S10.** Cyclic voltammograms of methanol solutions containing 0.1 mM  $\text{LiCo}(\text{PDC})_2$ .  $\text{TBABF}_4$  was co-dissolved in the solution as an additive. The scan rate was  $100 \text{ mV}\cdot\text{s}^{-1}$ .



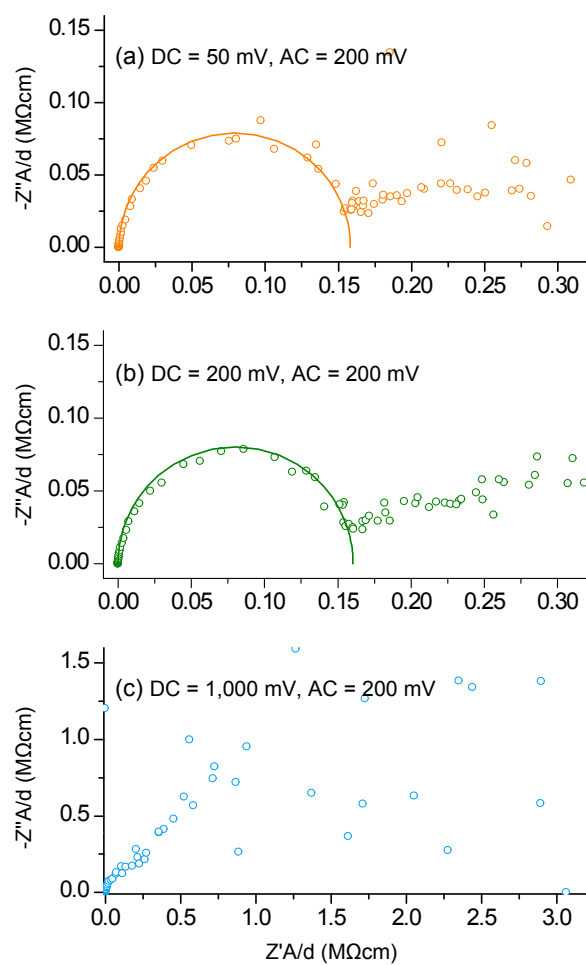


**Figure S11.** Measured (open circles) and simulated (solid curves) electrochemical impedance spectra of a  $\text{LiCo}(\text{PDC})_2$  single crystal sample connected to silver microelectrodes in the direction of [010]. The measurements were performed under various DC potentials: (a) 50, (b) 200, and (c) 1,000 mV. The AC potential was fixed at 200 mV.

**Table S5.** Conductivities of  $\text{LiCo}(\text{PDC})_2$  Samples

Sample	DC potential <sup>a</sup> (mV)	$R$ ( $\text{M}\Omega \text{ cm}$ )	$\sigma$ ( $\mu\text{S cm}^{-1}$ )	Ratio
Bulk pellet	400	26.1	0.0383	1
Single crystal in the [010] direction	50	0.159	6.27	164
	200	0.163	6.12	160
	1000	-	-	-

<sup>a</sup>Measurements were performed at a fixed AC potential of 200 mV.

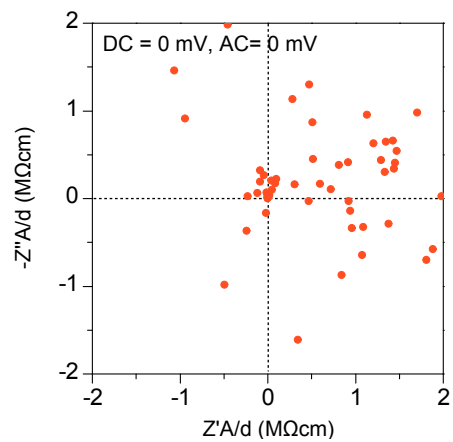


**Figure S12.** The impedance spectrum of a  $\text{LiCo}(\text{PDC})_2$  single crystal sample connected to silver microelectrodes in the direction of [010]. The measurement was performed without applied potential.

## Section S9. Conductivity Measurements of $\text{ACo(PDC)}_2$ ( $\text{A} = \text{Na}^+$ , $\text{K}^+$ , and $\text{H}_3\text{O}^+$ ) Single Crystals

As described in the text, we predicted that no ion conduction would be observed in the single crystals of  $[\text{H}_3\text{O}]\text{Co(PDC)}_2$ ,  $\text{NaCo(PDC)}_2$ , and  $\text{KCo(PDC)}_2$  because of the absence of ion channels (in the  $\text{NaCo(PDC)}_2$  crystal) or the strong binding of cations ( $\text{H}_3\text{O}^+$  and  $\text{K}^+$ ) to the surrounding oxygen atoms (in both the  $[\text{H}_3\text{O}]\text{Co(PDC)}_2$  and  $\text{KCo(PDC)}_2$  crystals). To demonstrate this prediction, we prepared large single crystal samples connected in the  $[100]$ ,  $[010]$ , and  $[001]$  directions and subjected the samples to EIS measurements. In all experiments, we did not observe an impedance signal. All data points in the spectra were completely scattered. Figure S13 shows typical impedance spectra recorded from the  $[\text{H}_3\text{O}]\text{Co(PDC)}_2$ ,  $\text{NaCo(PDC)}_2$ , and  $\text{KCo(PDC)}_2$  single crystal samples.

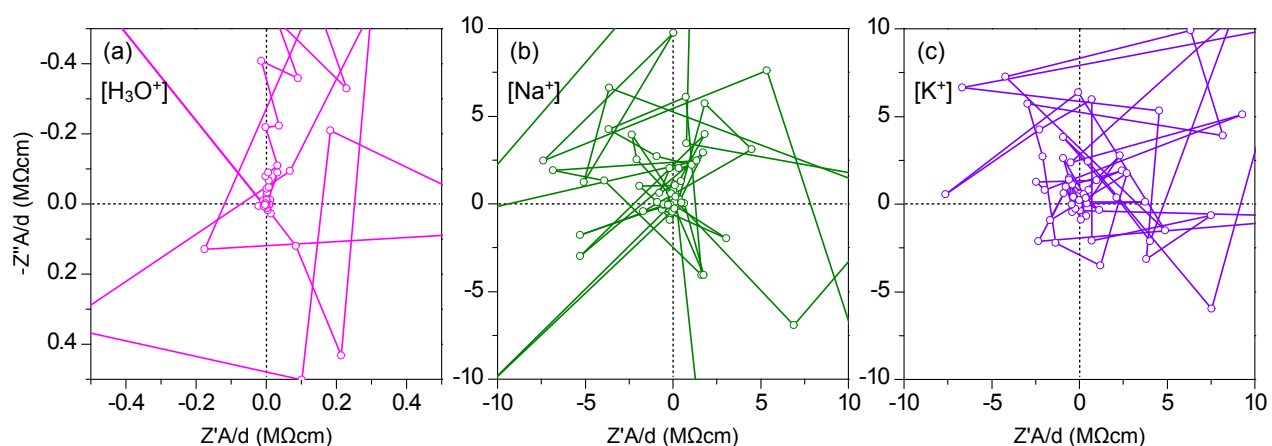


**Figure S13.** Typical impedance spectra of (a)  $[\text{H}_3\text{O}]\text{Co(PDC)}_2$ , (b)  $\text{NaCo(PDC)}_2$ , and (c)  $\text{KCo(PDC)}_2$  single crystals.

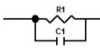
## Section S10. Identification of Conductivity in LiCo(PDC)<sub>2</sub>

Because the LiCo(PDC)<sub>2</sub> crystal contained occluded water molecules, the observed arcs in the impedance spectra may have been due to proton conduction, presumably via Grotthuss-type proton transfer between water molecules. To elucidate the origin of the arcs, the capacitance was extracted from the impedance spectra by fitting the spectra using Zview software. The dielectric constant ( $\epsilon_r$ ) was calculated according to the following equation:

$$C = \frac{\epsilon_r \epsilon_0 A}{d}$$

where  $C$ ,  $\epsilon_0$ ,  $A$ , and  $d$  are the capacitance, vacuum permittivity ( $8.85 \times 10^{-14}$  F·cm<sup>-1</sup>), area, and thickness of the sample, respectively. The calculated dielectric constant for a bulk pellet and single crystal is 4163 units and 1001–1125 units, respectively, substantially greater than the reported dielectric constant of water, ca. 80 units (see Table S6).<sup>S10</sup> Thus, the arcs obtained in the impedance spectra are attributable to the transport of Li<sup>+</sup> ions rather than the occluded water molecules. Because such high dielectric constants (>100) are frequently observed in coordination polymers (including MOFs)<sup>S11-13</sup> and ferroelectric materials,<sup>S14-15</sup> the high value of the extracted dielectric constant can be tentatively ascribed to the interaction of the Li<sup>+</sup> ion with the cobalt-PDC complex.

**Table S6.** Capacitances and Dielectric Constants Extracted from the EIS Spectra of the Samples.

Sample	$A/d$ (cm)	Applied AC Potentials (mV)	Capacitor component	Capacitance (F)	$\epsilon_r$
Bulk H <sub>2</sub> O (Reference) <sup>S10</sup>	–	–	–	–	80
LiCo(PDC) <sub>2</sub> : bulk pellet	2.1380	400	C <sub>1</sub>	$2.56 \times 10^{-10}$	1352
		400	C <sub>2</sub>	$2.88 \times 10^{-10}$	1521
		(C <sub>n</sub> = C <sub>1</sub> +C <sub>2</sub> )	C <sub>n</sub>	$5.44 \times 10^{-10}$	2874
		LiCo(PDC) <sub>2</sub> : [010] axis	0.0079	150	C <sub>1</sub>
		200	C <sub>1</sub>	$6.96 \times 10^{-13}$	1001
		250	C <sub>1</sub>	$7.82 \times 10^{-13}$	1125
		300	C <sub>1</sub>	$7.43 \times 10^{-13}$	1069
		350	C <sub>1</sub>	$7.10 \times 10^{-13}$	1022
		400	C <sub>1</sub>	$8.76 \times 10^{-13}$	1260

## Section S11. Temperature-dependent Conductivity Measurements for $\text{LiCo}(\text{PDC})_2$

To determine an activation energy required for the transport of  $\text{Li}^+$  ion residing in the small channel space of  $\text{LiCo}(\text{PDC})_2$  crystal, we examined the temperature-dependent conductivity using a  $\text{LiCo}(\text{PDC})_2$  pellet. The result indicated that the conductivity increased as the temperature increased (see Figure S14). This conductivity change was well fitted to an Arrhenius plot and the activation energy was calculated to be 0.47 eV (see Figure S15). We note that the activation energy is approximately 20-fold higher than a theoretical thermal energy corresponding to room temperature (ca. 25.7 meV). Although more comprehensive study is required to address this point, we observed that the activation energy is comparable to the values obtained from other porous materials.<sup>S16-S17</sup> We also observed that the values of capacitance and dielectric constant calculated from the Nyquist plots of this experiments were agreed well with the values obtained from other samples used in Section S10.

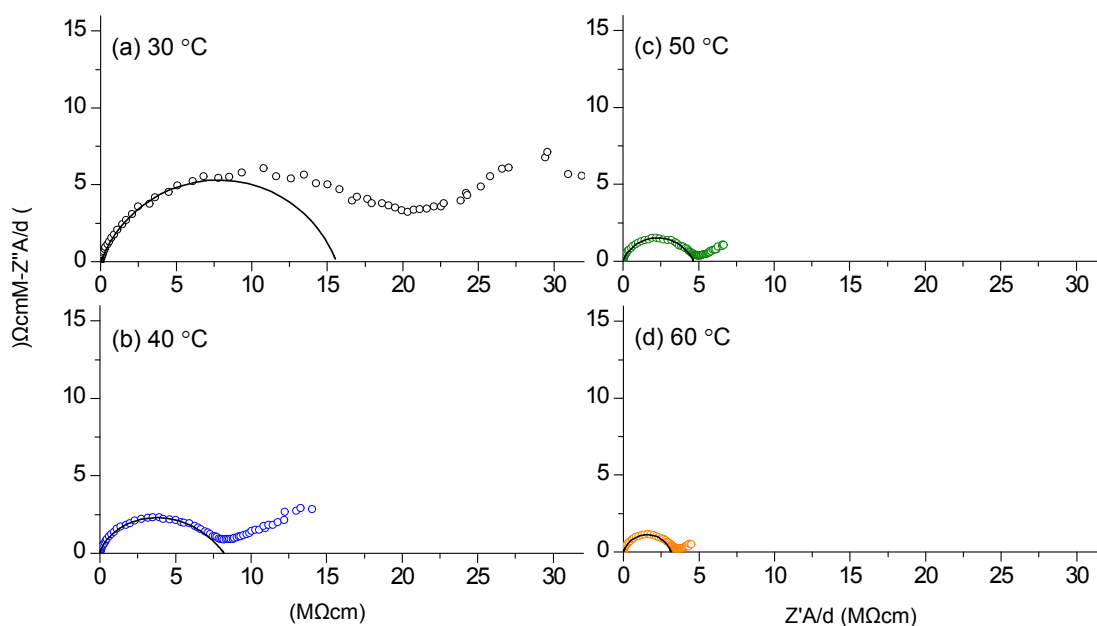


**Figure S14.** Nyquist plots of  $\text{LiCo}(\text{PDC})_2$  pellet measured at different temperatures. Solid curves indicate the fitting results for the corresponding Nyquist plots.

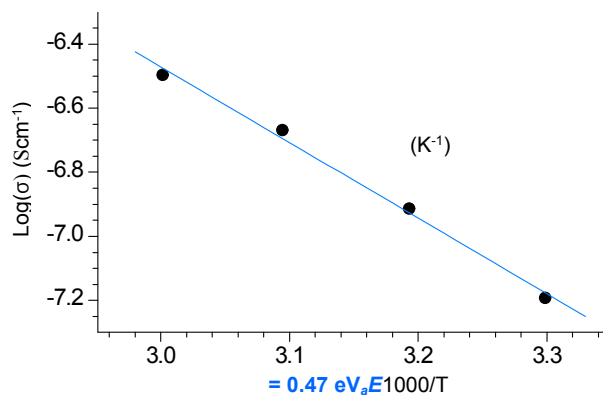


**Figure S15.** Arrhenius plot based on the conductivity measurements for  $\text{LiCo}(\text{PDC})_2$  pellet. Activation energy was obtained by least-square fitting (solid line) as indicated.

## References

- S1. SAINT. *Siemens Analytical X-ray Instruments, Madison, WI, 1995.*
- S2. Farrugia, L. *J. Appl. Crystallogr.* **1999**, *32*, 837.
- S3. Sheldrick, G. *University of Göttingen, Germany 1997*, 97-2.
- S4. Sheldrick, G., SHELXL-97, program for X-ray crystal structure refinement. University of Göttingen, Germany: **1997.**
- S5. Jeon, H. R.; Lee, D. W.; Ok, K. M. *J. Solid State Chem.* **2012**, *187*, 83-88.
- S6. Doadrio, A. L.; Sotelo, J.; Fernández-Ruano, A. *Química Nova* **2002**, *25*, 525-528.
- S7. Harada, H.; Kodera, M.; Vučković, G.; Matsumoto, N.; Kida, S. *Inorg. Chem.* **1991**, *30*, 1190-1194.
- S8. Comba, P.; Sickmuüller, A. F. *Inorg. Chem.* **1997**, *36*, 4500-4507.
- S9. Kügler, M.; Gałęzowska, J.; Schendzielorz, F.; Dechert, S.; Demeshko, S.; Siewert, I. *Eur. J. Inorg. Chem.* **2015**, 2695–2706
- S10. Permittivity (Dielectric Constant) of Liquids. In *CRC Handbook of Chemistry and Physics*, 90th ed.; Lide, D. R., Ed. CRC Press: Boca Raton, FL, **2010**; p 6-149.
- S11. Qu, B. -T.; Lai, J. -C.; Liu, S.; Liu, F.; Gao, Y. -D.; You, X. -Z. *Cryst. Growth Des.* **2015**, *15*, 1707-1713.
- S12. Brede, F. A.; Heine, J.; Sextl, G.; Miller-Buschbaum, K. *Chem. Eur. J.* **2016**, *22*, 2708-2718.
- S13. Tang, Y. -Z.; Huang, X. -F.; Song, Y. -M.; Chan, P. W. H.; Xiong, R. -G. *Inorg. Chem.* **2006**, *45*, 4868-4870.
- S14. Homes, C. C.; Vogt, T.; Shapiro, S. M.; Wakimoto, S.; Ramirez, A. P. *Science* **2001**, *293*, 673-676.
- S15. Hughes, H.; Allix, M. M. B.; Bridges, C. A.; Claridge, J. B.; Kuang, X.; Niu, H.; Taylor, S.; Song, W.; Rosseinsky, M. *J. J. Am. Chem. Soc.* **2005**, *127*, 13790-3791.
- S15. Hughes, H.; Allix, M. M. B.; Bridges, C. A.; Claridge, J. B.; Kuang, X.; Niu, H.; Taylor, S.; Song, W.; Rosseinsky, M. *J. J. Am. Chem. Soc.* **2005**, *127*, 13790-3791.
- S16. Yamada, T.; Sadakiyo, M.; Kitagawa, H. *J. Am. Chem. Soc.* **2009**, *131*, 3144-3145.
- S17. Sadakiyo, M.; Yamada, T.; Kitagawa, H. *J. Am. Chem. Soc.* **2009**, *131*, 9906-9907.